# Computing the multifractal spectrum from time series: An algorithmic approach

K. P. Harikrishnan*
*Department of Physics, The Cochin College, Cochin-682 002, India*

R. Misra†
*Inter University Centre for Astronomy and Astrophysics, Pune-411 007, India*

G. Ambika
*Indian Institute of Science Education and Research, Pune-411 021, India*

R. E. Amritkar
*Physical Research Laboratory, Navarangapura, Ahmedabad-380 009, India*

arXiv:0910.3105v1 [nlin.CD] 16 Oct 2009

We show that the existing methods for computing the $f(\alpha)$ spectrum from a time series can be improved by using a new algorithmic scheme. The scheme relies on the basic idea that the smooth convex profile of a typical $f(\alpha)$ spectrum can be fitted with an analytic function involving a set of four independant parameters. While the standard existing schemes [18, 20] generally compute only an incomplete $f(\alpha)$ spectrum (usually the top portion), we show that this can be overcome by an algorithmic approach which is *automated* to compute the $D_q$ and $f(\alpha)$ spectrum from a time series for any embedding dimension. The scheme is first tested with the logistic attractor with known $f(\alpha)$ curve and subsequently applied to higher dimensional cases. We also show that the scheme can be effectively adapted for analysing practcal time series involving noise, with examples from two widely different real world systems. Moreover, some preliminary results indicating that the set of four independant parameters may be used as diagnostic measures is also included.

PACS numbers: 05.45.Ac, 05.45.Tp, 05.45.Df

**It is now well established that multifractal sets and objects abound in Nature. A characteristic feature of these objects is the self similarity since their formation is governed by subtle scaling laws. An important tool to analyse these sets is the $f(\alpha)$ spectrum which describes how the fractal dimensions of the interwoven sets with defnite singularity strength are distributed. In the recent issue of *Chaos*, participating in the discussion "Is the normal heart rate chaotic?", many authors [1, 2] stress the importance of multifractality in the study of heart rate variability and suggest that it can provide a new observational window into the complexity mechanism of heart rate control. The study also highlights the need for evaluating new nonlinear parameters for a better physiologcal investigation and for finding new clinical applications. Here we present a novel automated scheme to compute the $f(\alpha)$ spectrum of a multifractal from its time series. We show that the scheme can be applied to synthetic as well as practical time series involving noise. It also provides us with an additional set of two independant parameters apart from the conventional $\alpha_{min}$ and $\alpha_{max}$ to characterise any general $f(\alpha)$ curve. The utility of these parameters from the point of view of diagnostic measures is also pursued by analysing a few class of physiological time series.**

## I. INTRODUCTION

Multifractal sets and objects form the supporting structure of nonlinear phenomena, prime examples being strange attractors of chaotic dynamical systems [3, 4] regions of high vorticity in fully developed turbulence [5, 6, 7] and fractal growth patterns [8, 9]. Multifractal analysis has also been applied in a variety of other fields, such as, to describe the morphologic and hydrologic characteristics of river basins [10, 11] and to analyse the velocities of solar wind plasma in the inner heliosphere [12]. In the case of chaotic dynamical systems, their long time evolution takes place in a subset of the phase space called *strange attractors*, which are characterised by a spectrum of generalised dimensions $D_q$ [13] and the associated singularity spectrum $f(\alpha)$ [14, 15, 16]. The $f(\alpha)$ spectrum provides a mathematically precise and naturally intuitive description of the multifractal measure in terms of inter woven sets with singularity strength $\alpha$, whose fractal dimension is $f(\alpha)$.

For simple chaotic systems, such as one dimensional maps, $f(\alpha)$ spectrum can be determined analytically. To evaluate the $f(\alpha)$ spectrum from the time series, there are basically two methods. In the conventional method [17, 18], one first computes the $D_q$ spectrum from the time series and use the fact that the transformation from

*Electronic address: kp˙hk2002@yahoo.co.in
†Electronic address: rmisra@iucaa.ernet.in

$D_q$ to $f(\alpha)$ is a Legendre transformation determined by the equations [18, 19]

$$\alpha = \frac{d}{dq}[(q-1)D_q] \tag{1}$$

$$f(\alpha) = q\alpha - (q-1)D_q \tag{2}$$

However, such a procedure is generally considered to be very difficult when done subjectively, as it involves first smoothing the $D_q$ curve and then Legendre transforming. Moreover, the error bar from the smoothing procedure makes the estimation of $f(\alpha)$ more difficult and often, the complete spectrum cannot be recovered.

An alternative method has been proposed in the literature by Chhabra and Jensen [CJ] [20] for the evaluation of $f(\alpha)$ from a time series without resorting to the intermediate Legendre transform. In this method $f(\alpha)$ is computed directly from the slopes by plotting the normalised measures defined through probabilities as a function of logarithm of box size for different $q$ values. The method gives good results and is devoid of the difficulty of Legendre transforming in the conventional method. But here one needs to use an optimal covering of the measure and the subjective evaluation of the slopes can give rise to error bar directly in the $f(\alpha)$ curve. Both these methods generally compute only an incomplete $f(\alpha)$ spectrum (usually the top region) and the problem becomes worse for attractors of more than one dimension.

Here we propose an algorithmic approach to overcome these difficulties and compute the complete spectrum from the time series for any dimension. Our scheme is based on the idea that the typical convex profile of the $f(\alpha)$ spectrum can be fitted by an analytic function involving a set of parameters. This function can be inverted using Eqs. (1) and (2) to get a smooth $D_q$ curve, which can in turn be fitted to the $D_q$ spectrum computed from the time series. By changing the parameters, the statistically best fit $D_q$ curve is chosen from which the final $f(\alpha)$ spectrum can be evaluated. It should be noted that we are not proposing any new method, but a new algorithmic approach to improve the existing methods.

Our approach has several new features. It avoids many of the sources of error in the conventional method such as smoothing the $D_q$ curve and using the polynomial fit to recover the complete $f(\alpha)$ curve. Moreover, the whole procedure is made into an *automated* algorithmic scheme in the sense that once the time series is given, the scheme computes the $D_q$ and $f(\alpha)$ curves for the required embedding dimension without requiring any intermediate subjective analysis. Though the scheme is illustrated here for the conventional method, it can in principle be applied for the CJ method as well. The only difference is that the fit has to be performed directly on the $f(\alpha)$ spectrum computed from the time series rather than the $D_q$ spectrum.

Apart from the computation of the $f(\alpha)$ curve, another important outcome of our algorithmic approach is the result that any $f(\alpha)$ curve can, in general, be completely characterised with the help of four independant parameters including the conventional $\alpha_{min}$ and $\alpha_{max}$. From a practical point of view, this presents us with more options for representing the changes in the multifractal character of a system. Some preliminary results in this regard obtained from the analysis of a class of physiological time series is also included in the paper.

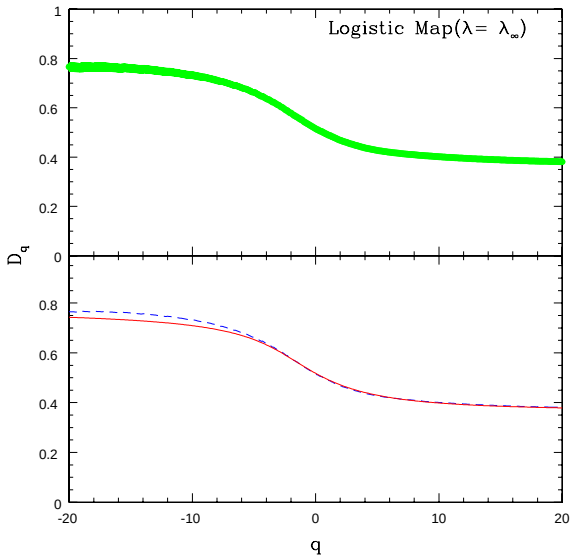



FIG. 1: The $D_q$ values, with error bar, of the strange attractor at the period doubling accumulation point of the logistic map calculated from the time series with 10000 data points are shown in the upper panel. To show the accuracy of fitting, these values are again plotted in the lower panel without error bar (dashed lines) along with the best fit curve (continuous line).

Our paper is organised as follows: the algorithmic scheme is discussed in detail in Sec.II. The scheme is then tested in Sec.III using the time series from logistic attractor at the period doubling accumulation point where, the $f(\alpha)$ curve is known theoretically. It is then applied to some other standard chaotic attractors in higher dimensions. Sec.IV considers the application of the scheme to practical time series, where the effect of noise on the $f(\alpha)$ spectrum is also studied. Discussions and conclusions are given in Sec.V.

## II. ALGORITHMIC SCHEME

### A. Computation of $D_q$

As the first step, the spectrum of generalised dimensions $D_q$ are computed from the time series using the delay embedding technique [21]. For this, an embedded space of dimension $M$ is constructed from the scalar time series $s(t_i)$ as

$$\vec{x_i} = [s(t_i), s(t_i+\tau), ...., s(t_i+(M-1)\tau)] \tag{3}$$

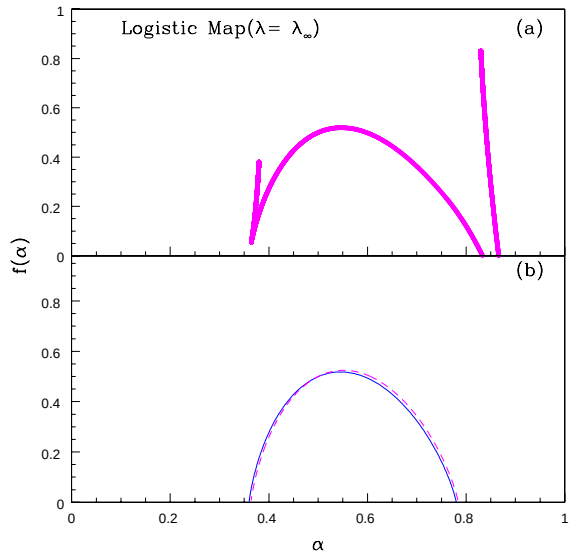



FIG. 2: (a)The $f(\alpha)$ spectrum of the logistic attractor obtained directly from the $D_q$ values which is incomplete. (b)The $f(\alpha)$ spectrum computed from the best fit curve (continuous line) in the previous figure along with the theoretical curve (dashed line). The agreement between the two is evident.

where $\tau$ is a suitably chosen time delay. The generalised correlation sum $C_q(R)$ is given by the relative number of data points within a distance $R$ from a particular ($i^{th}$) data point, say $c_i(R)$, raised to the power of $(q-1)$ and averaged over $N_c$ randomly selected centres:

$$c_i(R) = \frac{1}{N_v} \sum_{j=1, j\neq i}^{N_v} H(R - |\vec{x_i} - \vec{x_j}|) \tag{4}$$

$$C_q(R) = \frac{1}{N_c} \sum_{i}^{N_c} c_i(R)^{q-1} \tag{5}$$

where $N_v$ is the number of vectors. Then the spectrum of dimensions are given by

$$D_q \equiv \frac{1}{q-1} \lim_{R\to 0} \frac{\log\ C_q(R)}{\log\ R} \tag{6}$$

In practical considerations, $D_q$ is computed by taking the slope of $\log C_q(R)$ versus $\log R$ over a region of $R$ where the slope is nearly a constant i.e. a scaling region. For large $R$ (apart from the formal breakdown of the limit $R \to 0$), the slope does not represent $D_q$ since the M-spheres may extend outside the attractor, an effect known as "edge effect". For small $R$, the correlation sum is affected by counting statistics due to the finite length of the data stream. In general, the appropriate scaling region where both these effects are negligible is often chosen by subjective visual inspection. We have recently proposed an algorithmic scheme which non subjectively chooses an appropriate region [22]. The scheme which was developed to compute $D_2$, uses M-cubes instead of M-spheres and chooses only those centres where the M-cubes are inside the attractor region, thus avoiding the "edge effect". For large $R$, the number of such centres decrease and by the condition that at least $N_v/100$ centres are used for the computation, a maximum value of $R$, $R_{max}$ is obtained. To avoid the region dominated by counting statistics only results from $R > R_{min}$ are taken into considerations where $N_v C_2(R) > 10$, which ensures that on the average at least ten data points are being considered. The above estimation of the scaling region $R_{min} < R < R_{max}$ is adequate for computation of $D_2$ and the results obtained matches with theoretical values [22]. However, for the generalised correlation dimensions, there is an additional error which may occur for finite data sets. For large absolute values of $q$, the average over the randomly chosen centres Eq.(4) may be dominated by a few centres which have either large (for $q > 0$) or small (for $q < 0$) values of $c_i(R)$. This biases the result towards a few centres which may be due to statistical fluctuations. This effect is particularly strong when $q < 0$, where centres with statistically small values of $c_i(R)$ are the main contributors to $C_q(R)$. This is overcome by demanding that at least $1/10$ of the centres have a value of $c_i(R)^{q-1}$ greater than $C_q(R)$. This restricts the range of $R$ further and often a suitable range of $R$ is not available for small values of $q$. We fit a straight line to $\log C_q(R)$ versus $\log R$ for the range of $R$ that satisfy the above criteria and estimate $D_q$ from the slope of the best fit line. The standard error on the slope is used as an estimate of the error on $D_q$.

### B. Computation of $f(\alpha)$

Attempting to compute the $f(\alpha)$ spectrum directly from the $D_q$ values using Eqs. (1) and (2) leads to an incomplete $f(\alpha)$ spectrum (see Fig. 2a). This is mainly due to the fact that the errors in the calculation of $D_q$ makes the Legendre transforming numerically impractical because of reversal of slopes. The conventional method is to either smoothen the $D_q$ values or use a polynomial fit to recover the complete $f(\alpha)$ curve. Both can lead to large errors as has already been discussed by many authors. Here we follow a different procedure as given below.

The $f(\alpha)$ function is a single valued function defined between the limits of $\alpha_{min}$ and $\alpha_{max}$. Since the derivative $f'(\alpha) = df(\alpha)/d\alpha = q$ is also single valued, it follows that $f(\alpha)$ has a single extremum (i.e. a maximum). Moreover, $f(\alpha_{min}) = f(\alpha_{max}) = 0$ and $f'(\alpha_{min})$ and $f'(\alpha_{max})$ tend to $\infty$ and $-\infty$ respectively. A simple function which can satisfy all the above necessary conditions is

$$f(\alpha) = A(\alpha - \alpha_{min})^{\gamma_1}(\alpha_{max} - \alpha)^{\gamma_2} \tag{7}$$

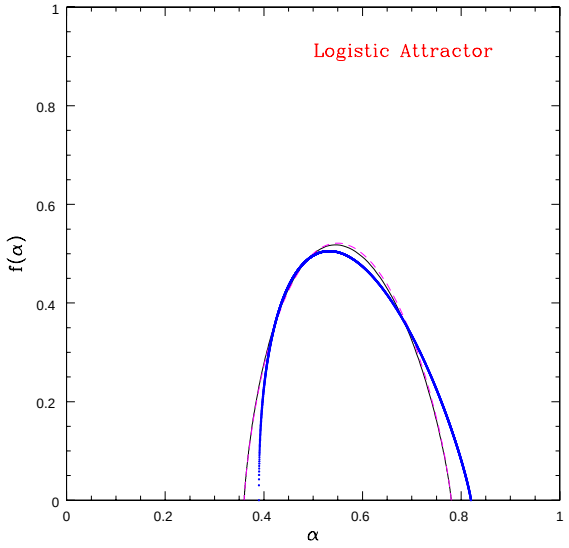



FIG. 3: The variation of the $f(\alpha)$ spectrum of the logistic attractor with number of data points. The spectrum almost completely coincide for 10000 data points (dashed line) and 5000 data points (solid line), but shows slight deviation as the number of data points are reduced to 3000 (thick line).

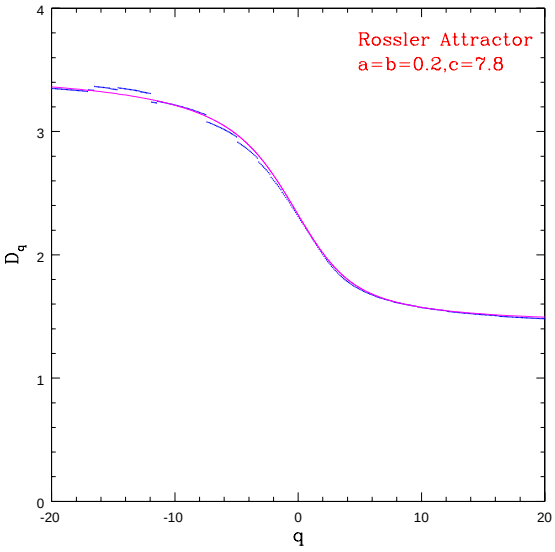



FIG. 4: The $D_q$ values (points) and its best fit curve (continuous line) for the Rossler attractor with 10000 data points computed using the scheme.

where $A$, $\gamma_1$, $\gamma_2$, $\alpha_{min}$ and $\alpha_{max}$ are a set of parameters characterising a particular $f(\alpha)$ curve. We will show that out of these five parameters, only four are independant which can unambiguously fix any general $f(\alpha)$ curve. From Eq. (2), we get

$$q = \frac{d}{d\alpha} f(\alpha) \tag{8}$$

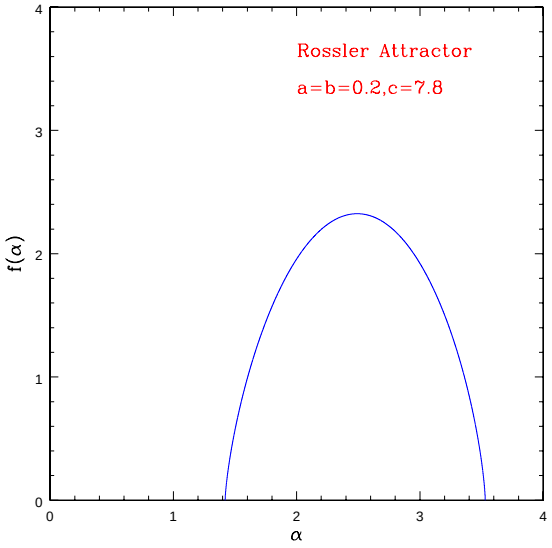



FIG. 5: The $f(\alpha)$ spectrum of the Rossler attractor computed from the best fit curve in Fig. (4).

Substituting for $f(\alpha)$ from above and simplifying

$$q = f(\alpha)\left[\frac{\gamma_1}{\alpha - \alpha_{min}} - \frac{\gamma_2}{\alpha_{max} - \alpha}\right] \tag{9}$$

The form of $f(\alpha)$ assumed in Eq. (7) implies that for it to be a well behaved function, $A$ should be positive and $\gamma_1, \gamma_2 > 0$. If $\gamma_1, \gamma_2 < 0$, then $f(\alpha) \to \infty$, as $\alpha \to \alpha_{min}, \alpha_{max}$. Imposing the condition that the slope of $f(\alpha)$ (that is, $\frac{d}{d\alpha} f(\alpha)$) should be $\infty$ at $\alpha = \alpha_{min}, \alpha_{max}$, we find from Eq. (9) that this is possible only if both $\gamma_1, \gamma_2 < 1$. Thus the range of $\gamma_1, \gamma_2$ should be restricted to

$$0 < \gamma_1, \gamma_2 < 1 \tag{10}$$

Corresponding to $q = 1$, there is a value of $\alpha(\equiv \alpha_1)$ and $f(\alpha)(\equiv f(\alpha_1))$ such that

$$D_1 = \alpha_1 = f(\alpha_1) \tag{11}$$

Putting $q = 1$ in Eq. (9), we get

$$\alpha_1\left[\frac{\gamma_1}{\alpha_1 - \alpha_{min}} - \frac{\gamma_2}{\alpha_{max} - \alpha_1}\right] = 1 \tag{12}$$

Using $\alpha_1, \alpha_{min}, \alpha_{max}$ and $\gamma_1$ as input parameters, $\gamma_2$ can be calculated from this equation. These values are then used to calculate the parameter $A$ from the original $f(\alpha)$ fit ($Eq.$ (7)) with $\alpha = \alpha_1(\equiv f(\alpha_1))$. Thus only four independant parameters are required to fix the $f(\alpha)$ curve.

The scheme first takes $\alpha_1(\equiv D_1), \alpha_{min}(\equiv D_\infty)$ and $\alpha_{max}(\equiv D_{-\infty})$ as input parameters from the computed $D_q$ values and choosing an initial value for $\gamma_1$ in the range $[0, 1]$, the parameters $\gamma_2$ and $A$ are calculated. The $f(\alpha)$ spectrum is then computed in the range $[\alpha_{min}, \alpha_{max}]$.

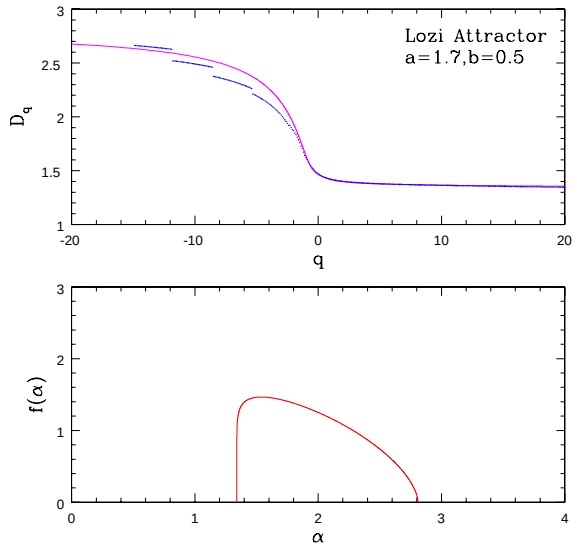



FIG. 6: The upper panel shows the $D_q$ values and its best fit curve (continuous line) for the Lozi attractor obtained by applying our numerical scheme. The corresponding $f(\alpha)$ curve is shown in the lower panel. Note that the $D_q$ branch for $q > 0$ is almost flat resulting in a highly asymmetric $f(\alpha)$ curve.

From this, the $D_q$ versus $q$ curve is then computed by inverting Eqs. (1) and (2) and fitted to the $D_q$ values computed from the time series.

A $\chi^2$ fitting is undertaken by changing the parameter $\gamma_1$ (which in turn changes $\gamma_2$ and $A$) untill the functional fit matches with the $D_q$ values from the time series in the best possible manner as indicated by the minimum of the $\chi^2$ value. The final $f(\alpha)$ spectrum is computed from the functional fit.

In the scheme, $D_1$ is used as one of the input parameters as it is obtained directly from the $D_q$ spectrum computed from the time series. But to represent the changes in the $f(\alpha)$ curve, it is more convenient to use $\gamma_1$ and $\gamma_2$ along with $\alpha_{min}$ and $\alpha_{max}$ as the free parameters. While $\alpha_{min}$ and $\alpha_{max}$ fix the end points of the spectrum (at which the slope becomes $\infty$), the values of $\gamma_1$ and $\gamma_2$ completely specify the nature of the $f(\alpha)$ profile. For example, as the difference between $\gamma_1$ and $\gamma_2$ increases, the spectrum becomes more and more asymmetric between the two branches. Moreover, they also determine the peak value of the spectrum $D_0$. If $\gamma_1 \sim \gamma_2 \sim 0$, then $D_0 \ll M$ and on the other hand, if $\gamma_1 \sim \gamma_2 \sim 1$, then $D_0 \sim M$. Thus the four parameters $\alpha_{min}, \alpha_{max}, \gamma_1$ and $\gamma_2$ can, in principle, completely characterise any $f(\alpha)$ spectrum.

## III. APPLICATION TO SYNTHETIC DATA

To test our scheme, it is first applied on the time series from the logistic attractor at the period doubling accumulation point, where the $f(\alpha)$ spectrum is known theoretically. The analysis is done with 10000 data points. The $D_q$ spectrum is first computed using Eq. (6) (with $M = 1$), for $q$ values in the range $[-20, +20]$. The computation is done taking a step width of $\Delta q = 0.1$. Choosing $D_{-20}, D_1$ and $D_{20}$ as the input values for the $f(\alpha)$ function Eq. 7, the parameters $\gamma_1$ and $\gamma_2$ are scanned in the range $[0, 1]$ untill the functional fit matches the $D_q$ values as indicated by the $\chi^2$ minimum. Since the error in $D_q$ generally bulges as $q \to -20$, the error bar is also taken into account in the fitting process. The $D_q$ values with error bar and the best fit curve are shown in Fig. 1. The complete $f(\alpha)$ spectrum computed from the best fit $D_q$ curve is shown in Fig. 2. For one dimensional maps, the $f(\alpha)$ curve can be determined theoretically [3]. To make a comparison, the theoretical $f(\alpha)$ curve is superimposed on the computed one in Fig. 2. Also shown in Fig. 2a is the incomplete $f(\alpha)$ spectrum computed directly from the $D_q$ values.

Since the $f(\alpha)$ spectrum for the logistic attractor is exactly known, it can also be used to test our scheme with respect to the number of data points required in a time series for a reasonable estimate of the $f(\alpha)$ spectrum. This is shown in Fig. 3, where the spectrum for the logistic attractor for three different number of data streams, namely, 3000, 5000 and 10000 are shown. It turns out that, a reasonable approximation to the $f(\alpha)$ spectrum can be obtained atleast with 3000 data points using our scheme in one dimension.

As the second example, we use time series generated from another standard chaotic attractor, namely, the Rossler attractor, for parameter values $a = 0.2, b = 0.2, c = 7.8$, with a time step of $\Delta t = 0.1$. The $D_q$ and $f(\alpha)$ spectrum are computed as above taking the total number of 10000 data points. The $D_q$ values and best fit curves for are shown in Fig. 4, while the $f(\alpha)$ curve is shown in Fig. 5.

In the above two cases, the $f(\alpha)$ curves are almost symmetric between the two branches. We now show that our scheme is also useful for the computation of more general types of $f(\alpha)$ curves. An example is that of the standard Lozi attractor. It is found that the $D_q$ spectrum in this case is almost flat for $q > 0$. But the $D_q$ spectrum can be accurately fitted by using the standard form of the $f(\alpha)$ function, as shown in Fig. 6. The corresponding $f(\alpha)$ spectrum computed from the best fit $D_q$ curve is also shown in Fig. 6 (lower panel), which turns out to be highly asymmetric between the two branches. While the parameter values $\gamma_1$ and $\gamma_2$ for the Rossler attractor are very close ($\gamma_1 = 0.65, \gamma_2 = 0.60$) as reflected in the nearly symmetric $f(\alpha)$ profile, that for Lozi attractor are completely different with $\gamma_1 = 0.09$ and $\gamma_2 = 0.60$. The scheme has also been applied to compute the spectrum of other standard chaotic attractors, such as, Henon and

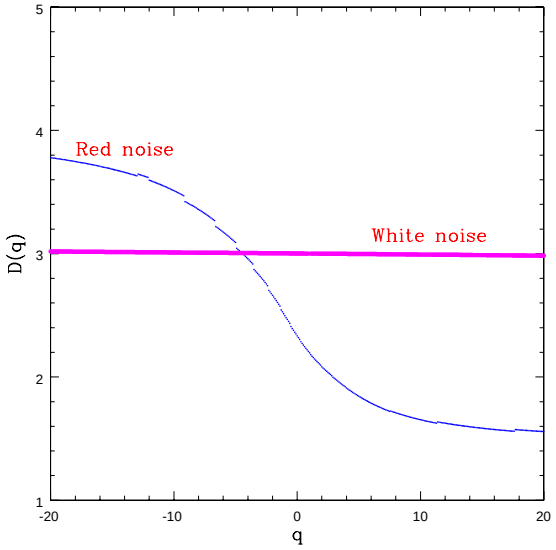



FIG. 7: The $D_q$ spectrum for white noise and red noise from 10000 data points. Note that the latter behaves like a chaotic system with a well defined $D_q$ curve.

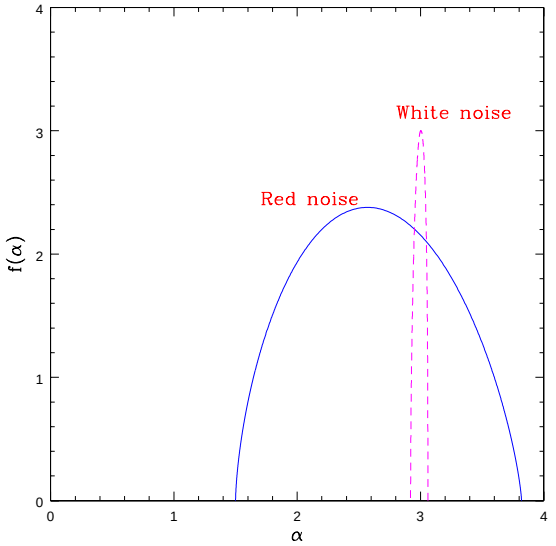



FIG. 8: The $f(\alpha)$ spectrum for white noise and red noise. The scheme accurately determines the $f(\alpha)$ spectrum of white noise which is expected to be a $\delta$ function corresponding to the embedding dimension.

Lorenz.

## IV. APPLICATION TO REAL WORLD DATA

Before the scheme is applied to practical time series, it is important to test it with time series involving noise. Since pure white noise is scale free, one expects the corresponding $f(\alpha)$ spectrum to be ideally a $\delta$ function with $f(\alpha) \equiv \alpha = M$, the embedding dimension. In Fig. 7, we show the $D_q$ spectrum of pure white noise and a colored noise with spectral index 2.0 (called *red noise*), computed from the respective time series for embedding dimension $M = 3$. The $f(\alpha)$ spectrum computed for both are shown in Fig. 8. While the $f(\alpha)$ spectrum of white noise is a $\delta$ function as expected, that of colored noise looks like a normal $f(\alpha)$ spectrum.

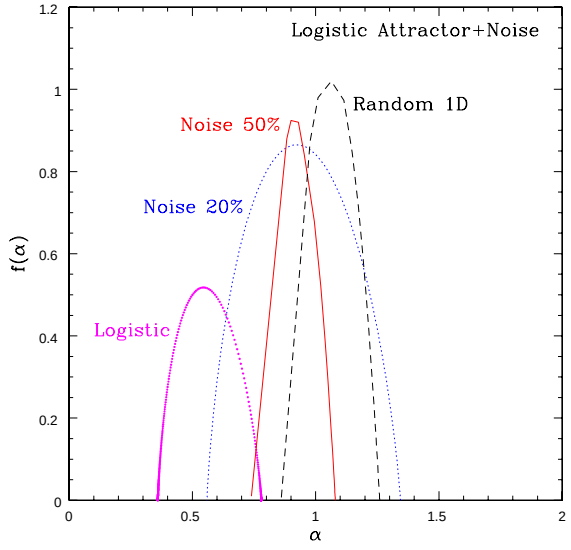



FIG. 9: Result of addition of white noise to the data from the logistic attractor. The $f(\alpha)$ spectrum for a noise level of 20% (dotted line) and 50% (solid line) are shown along with that of logistic attractor (points). The number of data points used for computation are 10000. Note that for 50% of noise contamination, the peak of the spectrum ($D_0$) almost touches the embedding dimension 1. For comparison, the $f(\alpha)$ spectrum of pure random noise in one dimension is also shown (dashed line).

To study the effect of noise on the $f(\alpha)$ spectrum of a chaotic attractor, we generate two time series by adding 20% and 50% white noise to the data from the logistic attractor using 10000 data points. White noise is used since it is scale free and hence can significantly alter the $f(\alpha)$ spectrum, while colored noise behaves much like a chaotic attractor with a well defined spectrum. Fig. 9 shows the $f(\alpha)$ spectrum of the logistic attractor added with 20% and 50% white noise, along with that of the logistic attractor. As the percentage of noise increases, the spectrum tends more and more towards a delta functon, centered around the embedding dimension $M = 1$. To get a proper comparison, the figure also shows the $f(\alpha)$ spectrum of pure random noise in one dimension.

We now apply our scheme to some real world data. We choose time series from two important fields, namely, astrophysics and physiology, where methods and concepts from nonlinear dynamics are constantly being applied. The first example is the X-ray light curve from a promi-

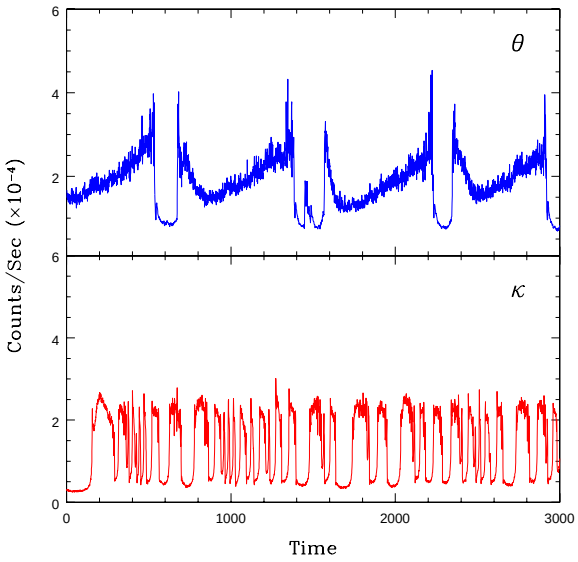



FIG. 10: A part of the light curves from two temporal states of the black hole system GRS1915+105.

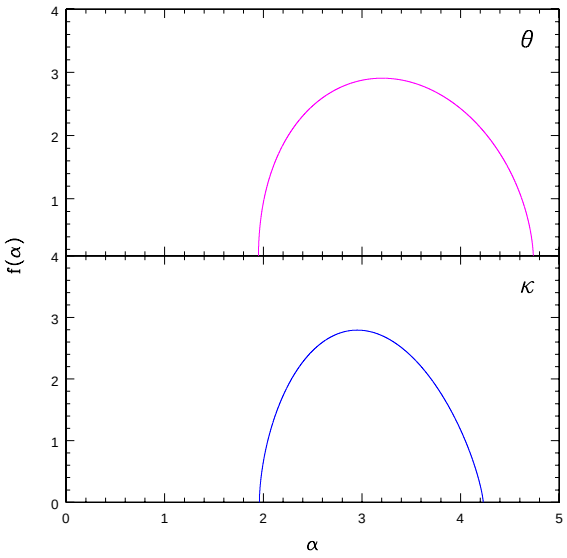



FIG. 12: The $f(\alpha)$ spectrum for the black hole states computed from the best fit $D_q$ curves in the previous figure.

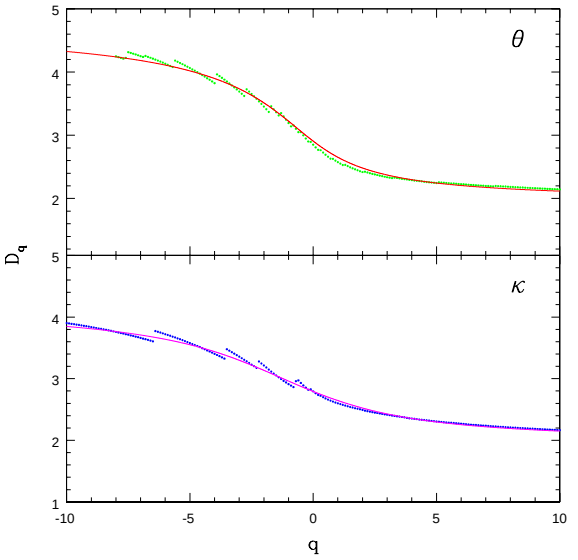



FIG. 11: The $D_q$ spectrum along with the best fit curve for the two states $\theta$ and $\kappa$ of the black hole system for embedding dimension $M = 3$.

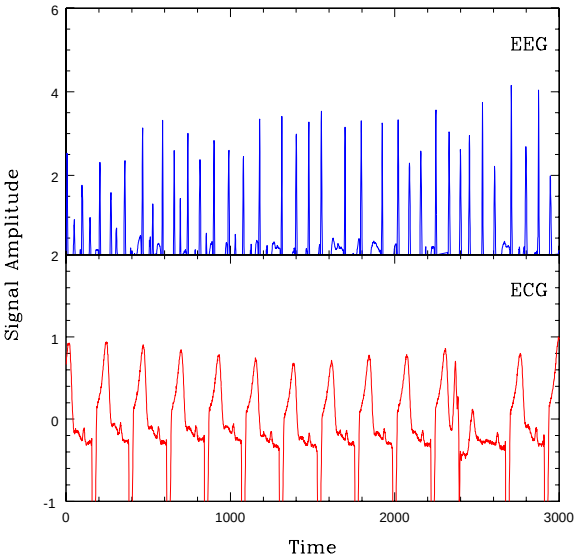



FIG. 13: A part of the EEG and ECG signals analysed in this work.

nent back hole binary, GRS1915+105. The light curves from this black hole system have been classified into 12 temporal states by Belloni et.al [23] based on RXTE observation. Here we choose data from two representative classes, $\theta$ and $\kappa$, and generate continuous light curves of approximately 6000 data points for both class. Fig. 10 shows a part of the light curves used for the analysis. Using surrogate analysis, we have recently shown [24, 25] that light curves from more than half of the 12 temporal states (including $\theta$ and $\kappa$) show significant deviation from stochastic behavior. The saturated value of correlation dimension for both are $< 3$. Hence $M = 3$ is chosen for applying our numerical scheme. The result of applying our scheme to the two light curves are shown in Fig. 11 and Fig. 12. The former shows the computed $D_q$ spectrum along with the best fit curve, while the latter shows the $f(\alpha)$ spectrum computed from the best fit curves. Note that, though the $D_q$ values are discontinuous for large negative $q$ values, one can statistically fit a smooth curve for $D_q$ from which the $f(\alpha)$ spectrum can be derived.

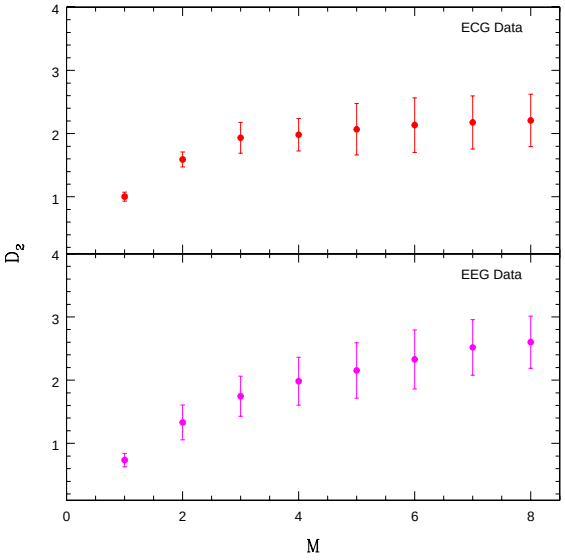



FIG. 14: The variation of correlation dimension $D_2$ (with error bar) as a function of $M$ for the EEG and ECG signals.

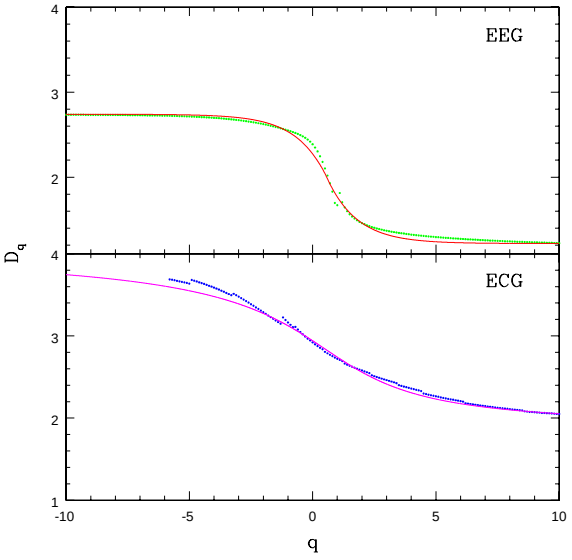



FIG. 15: The $D_q$ spectrum and the best fit curves for the EEG and ECG signals for $M = 3$.

As the second example, we use two data sets from physiology, namely an EEG data and an ECG data. The EEG data was downloaded from the website of the Department of Epileptology, University of Bonn while the ECG data was obtained from http://www.physionet.org/physiobank/archives. The EEG data is from an epileptic patient during seizure activity. The data consists of continuous data streams of about 24 seconds long and consisting of approximately 5000 data points. The ECG data was recorded from a heart patient with a congestive disorder and consists of continuous data streams of 5400 data points with a sampling time of 0.04 seconds. Both signals are shown in Fig. 13. First we compute the correlation dimension $D_2$ of both signals by applying the nonsubjective scheme [22] recently proposed by us, with the result shown in Fig. 14. For both signals, $D_2$ saturate well below $M = 3$. The results of applying our $f(\alpha)$ scheme are shown in Fig. 15 and Fig. 16, with multifractal character evident in both cases. Thus it is clear that the scheme can be successfully employed to compute the $D_q$ and $f(\alpha)$ spectrum from practical time series of finite data streams even with noise contamination, provided there exists an underlying chaotic attractor.

Finally, we would also like to stress the importance of computing the $f(\alpha)$ spectrum using an automated scheme, such as the one presented here. In the four examples of real world data that we have analysed above, the saturated $D_2$ values are approximately same, but the $f(\alpha)$ spectra are quite different. The subtle changes in the $f(\alpha)$ spectra can be better studied using the present scheme. This is because, the scheme provides an additional set of two independant parameters $\gamma_1$ and $\gamma_2$, apart from $\alpha_{min}$ and $\alpha_{max}$ which typically characterise

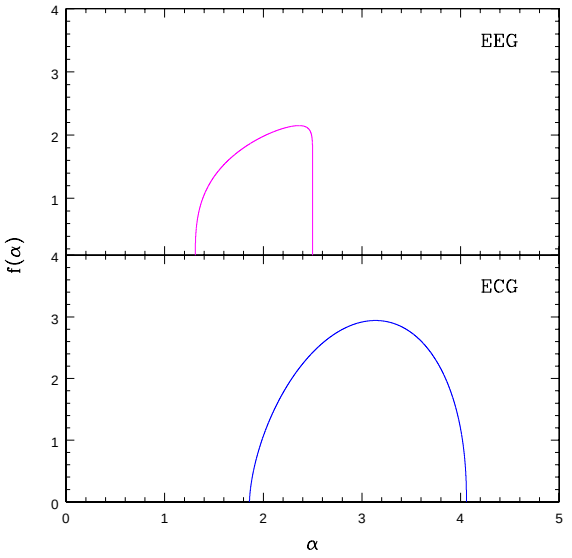



FIG. 16: The $f(\alpha)$ spectrum for the EEG and ECG signals computed from the best fit $D_q$ curves in the previous figure.

the changes in the $f(\alpha)$ profile. The utility of these parameters can be seen from Table I, which shows the result of a preliminary study made on some limited physiological time series. We have analysed four class of physiological data sets downloaded from the above mentioned websites. They are EEG and ECG signals from healthy human beings, EEG signal during epileptic seizure and ECG signals from patients with congestive heart failure. We have analysed five data streams for each class and Table I shows the average values of the two parameters $\gamma_1$ and $\gamma_2$ for each class along with $\alpha_{min}$ and $\alpha_{max}$,

TABLE I: The parameter values computed by our scheme for physiological data sets corresponding to four different class. The average values of five data streams for each class are shown.

| *Data Class* | $\alpha_{min}$ | $\alpha_{max}$ | $\gamma_1$ | $\gamma_2$ | $\lvert\gamma_1 - \gamma_2\rvert$ |
|---|---|---|---|---|---|
| EEG Healthy | $1.71 \pm 0.08$ | $4.18 \pm 0.17$ | $0.37 \pm 0.10$ | $0.32 \pm 0.14$ | 0.05 |
| EEG Epileptic Seizure | $1.28 \pm 0.06$ | $2.85 \pm 0.14$ | $0.34 \pm 0.08$ | $0.05 \pm 0.03$ | 0.29 |
| ECG Healthy | $1.46 \pm 0.12$ | $4.30 \pm 0.22$ | $0.69 \pm 0.08$ | $0.58 \pm 0.05$ | 0.11 |
| ECG Congestive Heart Failure | $1.88 \pm 0.10$ | $4.07 \pm 0.18$ | $0.29 \pm 0.06$ | $0.08 \pm 0.04$ | 0.21 |

with error bar showing the range of variation. We find that the values of $|\gamma_1 - \gamma_2|$ are significantly different for the healthy data and those with physiological disorder in both cases. Thus, just like $|\alpha_{max} - \alpha_{min}|$ which is conventionally used to characterise the geometric complexity of a multifractal, the quantity $|\gamma_1 - \gamma_2|$ may also be a potential candidate to quantify the inherent changes in the multifractal character of the system. Ofcourse, these results are only preliminary and have to be confirmed using a much larger number of data sets and requires an extensive analysis. Nevertheless, the initial results indicate that our scheme can be efficiently employed to quantify the changes in the multifractal character between various states of a complex system (such as the black hole system) or track changes in the $f(\alpha)$ spectrum arising out of various physiological disorder as reflected in the ECG or EEG time series, as shown here. We hope the scheme can be better utilised in this regard.

## V. DISCUSSION AND CONCLUSION

Computing the multifractal spectrum of a chaotic attractor from its time series is generally considered to be a difficult task. Often, only a part of the $f(\alpha)$ spectrum can be recovered numerically from the $D_q$ curve due to various reasons such as, the errors in the computation of $D_q$ and the Legendre transforming involved. Here we show that the existing methods can be improved using a new algorithmic approach by which the complete $f(\alpha)$ spectrum can be evaluated from a time series.

The scheme first assumes an analytical function for the $f(\alpha)$ curve, from which a functional fit for the computed $D_q$ values can be obtained by the inverse Legendre transform. The best fit curve is then used to derive the complete $f(\alpha)$ spectrum. The scheme is illustrated using time series from standard low dimensional chaotic systems and then applied to a variety of practical data from real world.

We have recently shown [26] that the the $f(\alpha)$ gives information only upto two scales evenif the underlying multiplicative process involves more than two. As a consequence, the $f(\alpha)$ spectrum of a chaotic attractor can, in general, be mapped onto that of a two scale Cantor set. This also provides an alternative method for computing the $f(\alpha)$ spectrum and to characterise a chaotic attractor in terms of the three independant parameters of a two scale Cantor set.

In contrast, an important aspect of the present scheme is that, an analytic function is proposed (which is probably unique) to fit all convex $f(\alpha)$ curves in general. Since the whole process is automated and the analysis is done under identical conditions prescribed by the algorithmic scheme, the resulting parameters characterising the spectrum (derived from a fitting function for $f(\alpha)$) give a better representation for comparison between data sets. This is especially important in the case of real world data since the changes in the same system, such as for example, due to some changes in the parameter, can be compared in a non-subjective manner.

In order to show this explicitely, the analysis of a few class of physiological data is also presented. We find that the subtle variations in the $f(\alpha)$ curve can be better characterised using our algorithmic scheme. Though our results indicate that the parameters may also be useful from a diagnostic point of view, this requires a much more comprehensive analysis using large number of data sets for confirmation. This is currently under way and will be presented elsewhere.

### Acknowledgments

The authors thank the Department of Epileptology, University of Bonn, for making the human brain EEG data available on their website.

KPH and RM acknowledge the financial support from Dept. of Sci. and Tech., Govt. of India, through a

Research Grant No. SR/S2/HEP - 11/2008.

KPH acknowledges the hospitality and computing facilities in IUCAA, Pune.

[1] R. Sassi, M. G. Signirini and S. Cerutti, Chaos **19**, 028507(2009).
[2] U. Freitas, E. Roulin, Jean-Francois Muir and C. Letellier, Chaos **19**, 028505(2009).
[3] R. C. Hilborn, *Chaos and Nonlinear Dynamics*, (Oxford University Press, New York, 1994).
[4] J. C. Sprott, *Chaos and Time Series Analysis*, (Oxford University Press, New York, 2003).
[5] B. B. Mandelbrot, J. Fluid Mech. **62**, 331(1974).
[6] R. Benzi, G. Paladin, G. Parisi and A. Vulpiani, J. Phys. A **17**, 352(1984).
[7] K. R. Sreenivasan and C. Meneveau, Phys. Rev. A **38**, 6287(1988).
[8] T. C. Halsey, P. Meakin and I. Procaccia, Phys. Rev. Lett. **56**, 854(1986).
[9] T. C. Halsey, Phys. Today **53**, 36(2000).
[10] A. Rinaldo, I. Rodriguez-Iturbe, R. Rigon, E. I. Vasquez and R. L. Bras, Phy. Rev. Lett. **70**, 822(1993).
[11] R. Rigon, A. Rinaldo and I. Rodriguez-Iturbe, J. Geophys. Res. **99**, 11971(1994).
[12] W. M. Macek, Phys. Rev. E **72**, 017202(2005).
[13] H. G. E. Hentschel and I. Procaccia, Physica D **8**, 435(1983).
[14] M. H. Jensen, L. P. Kadanoff, A. Lichaber, I. Procaccia and I. Stavos, Phys. Rev. Lett. **55**, 2798(1985).
[15] T. C. Halsey, M. H. Jensen, L. P. Kadanoff, I. Procaccia and B. I. Shraiman, Phys. Rev. A **33**, 1141(1986).
[16] K. J. Falconer, J. Theor. Prob. **7**, 681(1994).
[17] A. Arneodo, G. Grasseau and E. J. Kostelich, Phys. Lett. A **124**, 424(1987).
[18] P. Grassberger, R. Badii and A. Politi, J. Stat. Phys. **51**, 135(88).
[19] H. Atmanspacher, H. Scheingraber and G. Wiedenmann, Phys. Rev. A **40**, 3954(1989).
[20] A. Chhabra and R. V. Jensen, Phys. Rev. Lett. **62**, 1327(1989).
[21] P. Grassberger and I. Procaccia, Physica D **9**, 189(1983).
[22] K. P. Harikrishnan, R. Misra, G. Ambika and A. K. Kembhavi, Physica D **215**, 137(2006).
[23] T. Belloni, M. Klein-Wolt, M. Mendez, M. van der Klis and J. van Paradijs, Astron. and Astrophys. **355**, 271(2000).
[24] R. Misra, K. P. Harikrishnan, B. Mukhopadhya, G. Ambika and A. K. Kembhavi, Astrophys. J. **609**, 313(2004).
[25] R. Misra, K. P. Harikrishnan, G. Ambika and A. K. Kembhavi, Astrophys. J. **643**, 1114(2006).
[26] K. P. Harikrishnan, R. Misra, G. Ambika and R. E. Amritkar, submitted to Physica D.